Ascenzi, I. Biddittu, P. F. Cassoli, A. G. Segre, E. Segre-Naldini, *J. Hum. Evol.* **31**, 409 (1996)], which if confirmed (both the date and the taxonomic assignation) would represent the coexistence of two different hominid species in Europe.
9. C. B. Stringer, *ibid.* **12**, 731 (1983); C. B. Stringer, in *Ancestors: The Hard Evidence*, E. Delson, Ed. (Liss, New York, 1985), pp. 289–295; C. B. Stringer, in *Aux Origines des* Homo sapiens, J. J. Hublin and A. M. Tillier, Eds. (Presses Universitaires de France, Paris, 1991), pp. 49–74.
10. I. Tattersal, *The Last Neanderthal* (Macmillan, New York, 1986).
11. A. Rosas, J. M. Bermúdez de Castro, E. Aguirre, *L'Anthropologie* **95**, 89 (1991); J. L. Arsuaga, I. Martínez, A. Gracia, J. M. Carretero, E. Carbonell, *Nature* **362**, 534 (1993); J. L. Arsuaga *et al.*, *Rev. Esp. Paleontol.* **nº Extraord.**, 269 (1996); J. L. Arsuaga, I. Martinez, A. Gracia, C. Lorenzo, *J. Hum. Evol.*, in press.
12. A. Rosas and A. Buscalioni, *Rev. Esp. Paleontol.* **12**, 23 (1997); A. Rosas, in *Atapuerca y Evolución Humana*, E. Aguirre, Ed. (Fundación Ramón Areces, Madrid, in press); J. M. Bermúdez de Castro, M. E. Nicolás, J. Rodríguez, in *ibid.*
13. P. Andrews, in *The Early Evolution of Man with Special Emphasis on Southeast Asia and Africa*, P. Andrews and J. L. Franzen Eds. (Courier Forsch.-Inst. Senckenberg: Frankfurt a. M., 1984), pp. 167–175; C. B. Stringer, in *ibid.*, pp. 131–143; B. A. Wood, in *ibid.*, pp. 99–111.
14. ATD6-15 minimum frontal breadth and bistephanic breadth is 95 to 100 mm and 100 mm, respectively. These sizes are well above those of ER 3733, ER 3883, Sangiran 2, or Trinil (all skulls with cranial capacities below 1000 cm^3). In spite of its thin frontal squama and delicate supraorbital torus, ATD6-15 was initially considered to be an adolescent because of its extensive frontal sinuses (*3*); however, because WT 15000 also shows a well-developed frontal sinus, ATD6-15 could well have belonged to an individual of similar age at death (around 11 years old), maybe the same individual as the ATD6-69 face.
15. The mylohyoid groove maintains with the alveolar margin a fairly low angle of about 34°. The only other fossil *Homo* mandible that approximates the form of the ATD6-5 mylohyoid groove is that of WT-15000. In the European middle Pleistocene hominids and Neandertals, the groove lies farther behind M3, and has an angle of 52° to 57° (mean of 12 is 54.9°).
16. A. Rosas, *J. Hum. Evol.* **28**, 533 (1995).
17. This morphology probably derives from the presumed primitive condition 2R: M + D of the apehominid clade, which characterizes some early Pleistocene hominids from the Koobi Fora region [B. A. Wood, S. A. Abbott, H. Uytterschaut, *J. Anat.* **156**, 107 (1988)].
18. The molars from TD6 are included in the category of hypotaurodontism [J. C. Shaw, *J. Anat.* **62**, 476 (1928)]. The trend to the total fusion of the roots leads to the meso and hypertaurodontism which seems to be a derived condition of *H. heidelbergensis* and *H. neanderthalensis*.
19. The identification of the postcranial remains was made by J. M. Carretero, A. Gracia, and C. Lorenzo.
20. Age at death was estimated using values for predicting age from stages of permanent tooth formation presented in tables 9 and 10 of B. H. Smith [in *Advances in Dental Anthropology*, M. A. Kelley and C. S. Larsen Eds. (Wiley-Liss, New York, 1991), pp. 143–168].
21. We dedicate this paper to Emiliano Aguirre, pioneer of the systematic excavations and research in the Sierra de Atapuerca. The excavations in the Sierra de Atapuerca are supported by the Junta de Castilla y León, and the Research Project by the Ministerio de Educación y Cultura (DGICYT, project no. PB93-0066-C03, and Unidad Asociada Atapuerca). We thank the Atapuerca research team. Special thanks are given to those who have excavated the Aurora stratum from TD6. We are also grateful to I. Tattersall, J. Schwartz, J. Rodríguez, E. Nicolás, J. van der Made, and three anonymous reviewers for comments on the manuscript. The human fossils were restored by P. Gutiérrez del Solar and B. Gómez-Alonso.

6 February 1997; accepted 15 April 1997

Tin-Based Amorphous Oxide: A High-Capacity Lithium-Ion–Storage Material

Yoshio Idota, Tadahiko Kubota, Akihiro Matsufuji, Yukio Maekawa, Tsutomu Miyasaka*

A high-capacity lithium-storage material in metal-oxide form has been synthesized that can replace the carbon-based lithium intercalation materials currently in extensive use as the negative electrode (anode) of lithium-ion rechargeable batteries. This tin-based amorphous composite oxide (TCO) contains Sn(II)-O as the active center for lithium insertion and other glass-forming elements, which make up an oxide network. The TCO anode yields a specific capacity for reversible lithium adsorption more than 50 percent higher than those of the carbon families that persists after charge-discharge cycling when coupled with a lithium cobalt oxide cathode. Lithium-7 nuclear magnetic resonance measurements evidenced the high ionic state of lithium retained in the charged state, in which TCO accepted 8 moles of lithium ions per unit mole.

Lithium-ion insertion materials have gained considerable attention because they can be used as an active electrode in Li-ion rechargeable batteries, which have potential applications ranging from portable electronic devices to electric vehicles. Until 1980, Li metals and alloys were used as anode (negative electrode) materials in combination with various solid-solution cathode materials (*1*) in Li-ion batteries. From 1985 onward, the sole alternative to the Li metal anode, adopted to overcome safety problems, were carbon-based Li-ion intercalation materials (*2*), which introduced the concept of a "rocking-chair" type of rechargeable battery. Lithium ions are reversibly stored between layered carbon frameworks, which thereby develop an electrochemical potential relative to the Li/Li^+ anode low enough to act as negative electrodes. There have been important improvements in the Li-storage capacity of carbon materials that allow it to exceed the stoichiometric limit of Li-ion intercalation in graphite (LiC_6), 372 milliampere-hours per gram (mA·hour/g) of C_6 (*3*). The possibility of creating high-capacity anodes that leapfrog this limit has been demonstrated with the deep doping of Li (*4*, *5*). A significant trade off occurs, however, with regard to the ability to guarantee the safety of high-capacity anodes after repeated charge-discharge operations, which often cause the formation of hazardous metallic Li (dendrite) on the electrode surface (*6*).

We have synthesized an amorphous metal-oxide material that can store Li ions with a Coulombic capacity reaching that of hydrogen-storage alloys, ensuring protection against dendritic Li formation. The amorphous material is a metal composite oxide glass that contains tin(II) oxide as an active center for Li adsorption. It provides a gravimetric capacity of >600 mA·hour/g (0.022 mol of Li per gram) for reversible Li adsorption and release, which corresponds in terms of reversible capacity per unit volume to more than 2200 mA·hour/cm^3 (0.075 mol of Li per cubic centimeter). The latter value is about twice the reversible capacity of state-of-the-art high-capacity carbon materials (840 to 1200 mA·hour/cm^3) (*5*).

The tin-based composite oxide (TCO) active material has a basic formula represented by SnM_xO_y, where M is a group of glass-forming metallic elements whose total stoichiometric number is equal to or more than that of tin ($x \geq 1$) and is typically comprised of a mixture of B(III), P(V), and Al(III). In the oxide structure, Sn(II) forms the electrochemically active center for Li insertion and potential development, and the other metal group provides an electrochemically inactive network of –(M–O)– bonding that delocalizes the Sn(II) active center. To confer high reversibility in Li storage and release, the Sn-O framework was thus anisotropically expanded by incorporating glass-forming network elements—B, P, and Al—in view of the enhancement of Li-ion mobility in the anisotropic glass structure, favorable

Y. Idota and T. Kubota, Fujifilm Celltec, Matsuzakadaira 1–6, Taiwa-cho, Kurokawa-gun, Miyagi 981–34, Japan. A. Matsufuji, Y. Maekawa, T. Miyasaka, Ashigara Research Laboratories, Fuji Photo Film, Nakanuma 210, Minamiashigara, Kanagawa 250–01, Japan.

*To whom correspondence should be addressed.

for ionic diffusion and release. For synthesis, powders of SnO, B_2O_3, $Sn_2P_2O_7$, and Al_2O_3 were mixed and grained at a molar ratio of Sn:B:P:Al = 1.0:0.6:0.4:0.4. The powder mixture was heated to 1100°C for more than 10 hours in an alumina crucible under flowing argon to invoke the reaction in a molten state. The resulting product was then quenched to room temperature at a cooling rate of 10° to 20°C per minute to yield a transparent yellowish glass. The glassy material has the formula $Sn_{1.0}B_{0.56}P_{0.40}Al_{0.42}O_{3.6}$ (named TCO-1), as analyzed by inductively coupled plasma atomic emission spectrometry. Active materials of various element ratios were also prepared in the same manner and were milled to yield white powders (Fig. 1).

Our x-ray diffraction analysis for the powders of TCO products established the noncrystalline (amorphous) state of these glassy materials (Fig. 2). A broad band of weak diffraction was observed, peaking at around $2\theta = 27°$ to 28°, without concomitance of any diffraction line assigned to crystalline forms. This distribution is characteristic of SnO-based oxide glasses studied for SnO-SiO_2 systems (*7*). Radial distribution analysis shows that the broad peak corresponds to a radius range of 3.0 to 4.5 Å, attributable to statistical distribution of the Sn-Sn distance rather than the Sn-O distance (2.2 Å in SnO). Morphological analysis of TCO glass by scanning electron microscope and energy-dispersive x-ray spectroscopy techniques established the homogeneity of the glass composition that follows the starting mixtures. Structurally, TCO is supposed to consist of homogeneously and anisotropically dispersed Sn-O core sites surrounded by a random network array of B_2O_3, P_2O_5, and Al_2O_3. The density of TCO-1 was 3.70 g/cm^3, which is less than the theoretical value of 3.9 to 4.1 g/cm^3 calculated from a crystalline model and 60% greater than that of graphite (2.26 g/cm^3).

Fig. 1. Bulk tin-based composite oxide (TCO) active material (left). It is a yellowish transparent glass with a density of 3.7 g/cm^3. Crushing the glass provides a white powder of active material (right) capable of Li insertion for use in the negative electrode of Li-ion rechargeable batteries. The powder typically has a surface area of 0.6 m^2/g, as measured by the Brunauer, Emmett, and Teller (BET) technique.

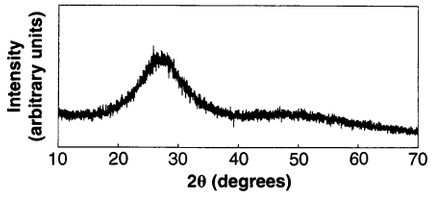

Fig. 2. The x-ray diffraction spectrum of TCO-1 under Cu Kα radiation. Only a weak diffraction distribution is observed with a peak at $2\theta = 27°$ to 28°, which is a characteristic of SnO-containing glass and reflects a distribution of Sn-Sn distances in the anisotropic matrix. The Li-absorbed charged state of TCO-1 gave essentially the same amorphous profile.

The Li storage capacity of TCO was investigated by means of electrochemical insertion of Li ions into TCO, with use of a button-type cell with a Li-metal counterelectrode (containing 6 mol % Al) serving as a Li-ion source. The TCO powder (average grain size of 5 to 10 μm) was mixed with a polytetrafluoroethylene (PTFE) powder as a binder and an electroconductive carbon powder in a weight ratio of 83:2:15, respectively, and was compressed into a pellet (thickness, 0.07 mm; area, 1.33 cm^2; weight of contained TCO, 20.8 mg). The TCO pellet and 0.6-mm-thick Li electrode were mounted in a button cell with a polypropylene separator sheet sandwiched between both electrodes. A nonaqueous electrolyte solution was used that consisted of ethylene carbonate (EC) and diethylcarbonate (DEC) in a volume ratio of 1:1; the electrolyte consisted of 1 mol of $LiPF_6$ per liter of solution. The cell was fabricated in a dry-air environment and was tightly shielded against ambient moisture.

The charge-discharge capacity of TCO was examined at room temperature. The cell was charged (Li inserted) to 0 V and discharged (Li released) to 1.20 V at a constant current of 1 mA. The curve (Fig. 3) shows that TCO working in the low-potential range (0 to 1.2 V versus Li/Li^+) is suitable for use as negative-electrode active material in Li-ion batteries. In the initial cycle, the charging capacity for Li-ion storage reached 1030 mA·hour/g, which corresponds to about 8 equivalent mole of Li ions per unit mole of TCO. Subsequent Li-release processes up to 1.2 V yielded a Coulombic capacity of 650 mA·hour/g (5 mol of Li released), accompanied by a 37% loss of the initial discharge efficiency (8). The latter capacity holds for succeeding cycles with nearly 100% Coulombic efficiency without causing a significant increase in electrode resistance.

The obtained reversible Li-ion storage capacity, >600 mA·hour/g, gives a specific capacity per unit volume of >2200 mA·hour/cm^3, which corresponds to nearly twice the level of existing state-of-the-art carbon materials (<1200 mA·hour/cm^3 and <500 mA·hour/g) (*3*). This extremely high capacity of TCO compares well with those capacities of hydrogen-storage alloys as represented by AB_5-type compounds such as $LaNi_5$. They give <2400 mA·hour/cm^3 (*9*) according to the stoichiometric limit of one atom of hydrogen for each atom of metal. In contrast, TCO is capable of accepting eight ions of Li per Sn atom,

Other TCO materials of different element molar ratios—Sn:B:P:Al such as 1.0:0.4:0.4:0.3, 1.0:0.5:0.5:0.4, 1.0:0.6:0.5:0.1, and 1.0:0.5:0.4:0.1—yielded essentially the same charge-discharge profile (*10*), although their Li storage capacities were dependent on the net content of Sn(II). The Sn–O bond apparently provides the core site that contributes to the active charge-discharge of Li species. Control materials free of Sn, comprising a glass-forming network of B, P, and Al only, gave substantially zero capacity (*11*).

Lithium-7 nuclear magnetic resonance measurements (^{7}Li-NMR) were conducted to elucidate the state of the Li ion inserted in the TCO. The ^{7}Li-NMR spectra of Li-inserted TCOs evidenced no single metallic bands in the course of cathodic charging of TCOs down to 0.06 V versus Li/Li^+. Figure 4A shows a typical ^{7}Li-NMR spectrum of TCO at a Li insertion level of Li/Sn = 8 [charging of 1000

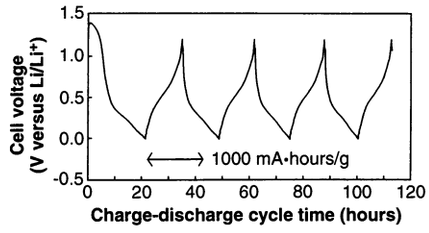

Fig. 3. Cycling of electrochemical Li insertion (charge) and release (discharge) on TCO-1 ($Sn_{1.0}B_{0.56}P_{0.40}Al_{0.42}O_{3.6}$) at a constant current of 1 mA per 20.8 mg of TCO-1, conducted at room temperature between the voltage limits of 0 V (insertion) and 1.2 V (release) versus a Li counterelectrode. The cell voltage and its limits are values monitored by the external circuit (they are not equivalent to OCV). The electrochemical cell comprised a TCO-mounted working electrode and Li counterelectrode dipped in an electrolyte composition containing EC and DEC (1:1) as solvents and $LiPF_6$ as the electrolyte. Data were extracted for the first four cycles. After the second cycle, insertion and release were entirely reversible, as the prolonged cycle test demonstrates (Fig. 5).

mA·hour/g, open circuit voltage (OCV) versus Li/Li^+ of 0.06 V]. This deep level of Li doping produced a chemical shift of 10 parts per million (ppm), small enough to assign the Li residing in the TCO matrix to a highly ionic state. We compared the NMR chemical shift of TCO with those of pure SnO and Sn metal (both in crystalline form) (Fig. 4B) as a function of the Li insertion depth (Li/Sn molar ratio); it is evident from the large chemical shifts that Li insertion into crystalline SnO of isotropic structure tends to form metallic Li to an extent close to the case of Sn-Li alloy formation in Sn metal.

On the basis of the above analysis, it is appropriate to look into the molecular structure of the Li-inserted state of TCO. It is considered that the participation of Li-ion coordination in reversible charge-discharge reactions takes place at the bonding orbital of Sn-O, accompanied by partial electronic reduction of both Sn(II) and Li^+, but not forming a state of metallic Li, as evidenced by ^{7}Li-NMR data (*12*). The chemical potentials of these Li ions, which determine their charge-discharge equilibrium potentials, may not be equivalent as a result of discrepancies in the Sn-Li separation and in the electronic densities of Sn and Li, both being affected by the surrounding metal oxide components. The anisotropic random network of the glass structure accounts for why there is a wide potential distribution in Li uptake and release as exhibited by the gentle slope in the charge-discharge curve (Fig. 3).

The charge-discharge cyclability of TCOs as anode materials of a practical "rocking-chair" type of rechargeable battery was assessed by adopting a $LiCoO_2$ electrode as a Li-intercalating cathode active material. In this test, a TCO anode with the composition $Sn_{1.0}B_{0.5}P_{0.5}Al_{0.4}M_{0.1}O_{3.7}$ was chosen, where M is an alkaline metal (such as potassium) mixed in the glass matrix as a dopant to reinforce cyclability (*13*). We prepared $LiCoO_2$ powder (average particle size, 6 μm) by calcining a powder mixture of Co_3O_4 and Li_2CO_3 (Co/Li molar ratio = 1.0) at 800°C for 8 hours and formed it into a conducting pellet with a PTFE binder and acetylene-black powder. The $LiCoO_2$-based cathode was combined with the TCO-based anode at an optimized mass ratio to effect Li insertion balance. The battery thus fabricated was subjected to a charge-discharge cycle over a voltage window between 4.1 and 2.8 V. This cycling test showed that 90% of the initial reversible capacity of the battery was retained after 100 cycles (Fig. 5). These results corroborate that, along with $LiCoO_2$, the TCO-based oxide anode performs highly reversible and stable charge-discharge reactions and is suitable as an anode in high-energy rechargeable batteries.

The large Coulombic capacity and good cyclic durability of TCO, backed by the safe Li-storage mechanism, provides a powerful tool in the design of rechargeable batteries whose capacity exceeds that of nickel hydride batteries (400 W·hours/liter) that use hydrogen-storage alloys of the largest capacity. The TCO anode can successfully be coupled with several available cathode active materials, including $LiCoO_2$, $LiNiO_2$, $LiMn_2O_4$, and $LiMnO_2$ (*14*). Using cylinder-type batteries with a series of TCO-based anodes and $LiCoO_2$ cathodes, we have thus far confirmed that batteries possessing an output voltage of 2.5 to 4.2 V, an energy density of 420 W·hours/liter, and good cyclic durability are feasible.

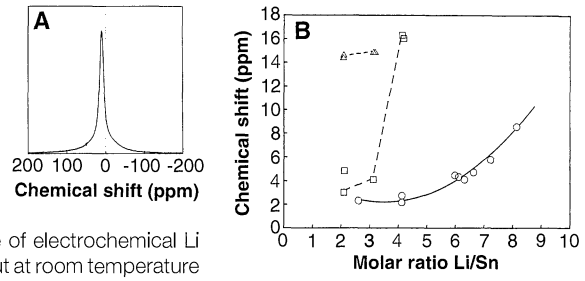

Fig. 4. (**A**) Nuclear magnetic resonance spectrum (NMR) of ^{7}Li for TCO after Li insertion to a molar ratio Li/Sn = 8. The Li was electrochemically inserted into TCO in the cell composition as in Fig. 1. (**B**) Chemical shifts of ^{7}Li-NMR spectra for TCO (○) and reference materials Sn metal (△) and SnO (□) as a function of Li/Sn molar ratio in the course of electrochemical Li insertion. Measurement was carried out at room temperature on a NSL-300 NMR spectrometer (Nippon Bruker) using LiCl as a standard. The results demonstrate the highly ionic state of Li being retained in TCO up to Li/Sn = 8, in contrast to Sn and SnO, which cause large chemical shifts.

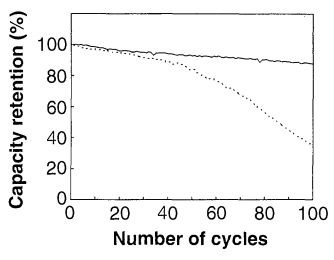

Fig. 5. Cyclability of a TCO (anode)/EC+DEC+$LiPF_6$/$LiCoO_2$ (cathode) "rocking-chair" type of battery (solid line). The battery was charge-discharge cycled over a cell-voltage window of between 4.1 V (charge) and 2.8 V (discharge) at a constant current corresponding to 0.5 C (*15*) (2 mA per 6.3 mg of discharged mass of TCO). In this cycling, voltage limits are controlled on the basis of OCV while charging and circuit voltage (including a voltage loss by net resistance) while discharging; the limit voltage of charge corresponds to 0.10 V versus Li^+/Li as the potential of the TCO anode. This result is compared with reference data (dashed line) for a similar battery in which the anode active material was replaced with a SnO powder, which, as revealed by the ^{7}Li-NMR experimental data (Fig. 4), lacks the ionic stability of Li.

REFERENCES AND NOTES

1. D. W. Murphy and P. A. Christian, *Science* **205**, 651 (1979).
2. R. Fong, U. Sacken, J. R. Dahn, *J. Electrochem. Soc.* **137**, 2009 (1990); B. Scrosati, *ibid.* **139**, 2776 (1992).
3. All specific capacity and capacity density values are expressed on the basis of unit mass or volume of the starting material (oxidized state) before Li insertion and exclude the mass of any Li in the weights of the anodic materials.
4. K. Sato, M. Noguchi, A. Demachi, N. Oki, M. Endo, *Science* **264**, 556 (1994).
5. S. Yata *et al.*, *Synth. Met.* **62**, 153 (1994).
6. Z. X. Shu, R. S. McMillan, J. J. Murray, *J. Electrochem. Soc.* **140**, 922 (1993). Effort has been made to design Li batteries without the use of Li-graphite anodes at low potentials [W. Li, J. R. Dahn, D. S. Wainwright, *Science* **264**, 1115 (1994)].
7. T. Ishikawa and S. Akagi, *Phys. Chem. Glasses* **19**, 108(1978).
8. The initial capacity loss is apparently brought on by an increase in the resistance of TCO in the course of discharge and depends on the discharge cut-off potential. Under discharge up to around 2 V versus Li/Li^+ (OCV), this loss is reduced to 25%, and further overvoltage recovers charge-discharge efficiency to the level of 85%. This fact indicates that the actual electrochemically irreversible portion in the initial Li-insertion reaction is one-seventh the initial charge capacity.
9. A. Anani *et al.*, *J. Power Sources* **47**, 261 (1994).
10. Some TCOs with low Sn content showed poor glass formability, as a sign that Sn itself serves as a glass-forming component.
11. We have found other glass-forming elements in metals and semi-metals such as Si, Ge, and V. Examples of other elements capable of constituting Sn-based oxide anodes, the optimization of which led to the invention of TCOs, are given in our patent applications: Y. Idota *et al.*, European Patent 651,450A1 (1995); *ibid.*, Canadian Patent 2,113,053 (1995); Y. Idota, U.S. Patent 5,478,671 (1995).
12. There is only limited evidence for the mechanism of irreversible Li insertion (efficiency loss). Because the anode is an oxide, the involvement of irreversible Li-oxygen interactions such as Li_2O formation must be considered first. As far as the ^{7}Li-NMR data of the charge-state TCO are concerned, however, we did not detect a definite mixing of the Li_2O species, which appear, when measured for a pure Li_2O sample, as a broad complex band (half width in chemical shift of 200 ppm centered near 0 ppm).
13. The effect of these dopants was discovered by random screening of glass-forming elements, and the exact chemical mechanism has not yet been determined. For detailed information, see K. Goda *et al.*, International Patent Application (PCT) WO96/33519.
14. A. R. Armstrong and P. G. Bruce, *Nature* **381**, 499 (1996).
15. Unit C represents the rate of charging (discharging) in which current is equivalent to the quantity of the nominal capacity of a battery, indicating the rate in which charging can be completed in essentially 1 hour if the rate efficiency is unchanged.

16. We gratefully acknowledge our colleagues at Fuji Photo Film: Y. Miyaki, M. Mishima, and K. Goda contributed to the synthesis and structural optimization of TCOs and Y. Kagawa, Y. Mineo, and H. Asanuma contributed to x-ray diffraction and ^{7}Li-NMR analysis.

25 November 1996; accepted 9 April 1997